PERGAMON

International Journal of Solids and Structures 38 (2001) 3719–3734

INTERNATIONAL JOURNAL OF SOLIDS and STRUCTURES

www.elsevier.com/locate/ijsolstr

Mixed-mode stress intensity factors for cracks located at or parallel to the interface in bimaterial half planes

H. Huang, G.A. Kardomateas *

School of Aerospace Engineering, Georgia Institute of Technology, Atlanta, GA 30332-0150, USA

Received 28 December 1999; in revised form 30 May 2000

Abstract

This paper presents a method for obtaining the mixed-mode stress intensity factors for bimaterial interface cracks or cracks parallel to the bimaterial interface in half-plane configurations. First, dislocation solutions in two different bimaterial half planes are presented. The boundaries of these two half planes are either parallel or perpendicular to the bimaterial interface. A surface dislocation model is employed to ensure the traction-free boundary conditions. The dislocation solutions are then applied to calculate the mixed mode stress intensity factors of cracks either at the interface or parallel to the interface. The effects of material mismatch, material interface, and boundary on the stress intensity factors are investigated extensively. © 2001 Elsevier Science Ltd. All rights reserved.

Keywords: Interface crack; Bimaterial; Anisotropic; Stress intensity factor; Mixed mode

1. Introduction

Bimaterials are extensively used in many engineered-material systems, such as composite structures, electronic packaging, and thin film constructions. Accurate stress intensity factor calculations are essential in the prediction of failure and the calculation of crack growth rates in these structures. A very effective method of determining stress intensity factors is the continuous dislocation technique. The cornerstone of this method is the fundamental solution of a dislocation in the corresponding configuration. Eshelby et al. (1953) and Stroh (1958) are among the pioneers who presented analytical solutions for a dislocation in general anisotropic materials. Following their work, Ting (1986) and Qu and Li (1991) studied the classical problem of a dislocation situated at the interface between two anisotropic elastic half planes and obtained an analytical solution to the dislocation problem. Atkinson and Eftaxiopoulos (1991) also achieved the solution for a dislocation in an anisotropic half plane and a bimaterial infinite plane, using the basic formulation of Stroh and appropriate image systems.

* Corresponding author. Tel.: +1-404-894-8198; fax: +1-404-894-2760.
E-mail address: gkardoma@mail.ae.gatech.ed (G.A. Kardomateas).

PII: S0020-7683(00)00245-6

Unlike homogeneous fully anisotropic materials, the analytical solution for a dislocation in a bimaterial half plane is unknown because of the material heterogeneity and the traction-free boundary conditions. All the afore-mentioned analytic dislocation solutions are restricted to bimaterial infinite planes. Dislocation solutions for bimaterial geometries with finite domains such as the half plane or the infinite strip are not available in the literature so far. Yet, several researchers investigated dislocations in homogeneous infinite strips and were able to achieve the traction-free boundary conditions by different techniques. Civelek and Erdogan (1982) developed a numerical method to calculate the dislocation solution in an isotropic homogeneous infinite strip by superposing the infinite plane with an additional elastic field, which is expressed by an airy stress function with Fourier transformation. Suo (1990) and Suo and Hutchinson (1990) extended this method to orthotropic materials and calculated the mixed-mode stress intensity factors for an infinite strip with semi-infinite cracks subjected to edge bending. A surface dislocation model was proposed by Jagannadham and Marcinkowski (1979) to calculate the stress fields of a finite body subjected to either applied stresses or an internal stress. Huang and Kardomateas (1999) developed a method to calculate the stress fields of a dislocation in a homogeneous anisotropic infinite strip and applied the solution to calculate the stress intensity factors for both single edge and double edge cracks in a fully anisotropic infinite strip. In addition, different finite element methods are also proposed to calculate the mixed-mode energy release rate for cracks or delaminations in cross-ply composite materials (O'Brien and Hooper, 1993; Qian and Sun, 1997; etc.).

In this paper, the analytic solution for a dislocation in an anisotropic bimaterial infinite plane is summarized first. The stress fields of a dislocation in two different types of bimaterial half planes are subsequently obtained by distributing a dislocation array along the traction free boundary of the half planes. These dislocation solutions are then applied to calculate the mixed-mode stress intensity factors of interface cracks or cracks parallel to the interface in both bimaterial half plane configurations. Some results of practical interest are presented.

2. Formulation

2.1. Dislocation solution in a bimaterial infinite plane

The analytical solution for dislocations in a bimaterial infinite plane has several different versions. Almost all of them originate from Stroh's formulation. Combining the solutions presented by Ting (1986), Qu and Li (1991) and Atkinson and Eftaxiopoulos (1991), we present first a concise summary of this elegant analytical solution for a dislocation in a bimaterial infinite plane.

The stress potentials for an anisotropic medium can be expressed as

$$\{\phi_i\} = \mathbf{B}\{f_\alpha(z_\alpha)\} + \bar{\mathbf{B}}\{\bar{f}_\alpha(\bar{z}_\alpha)\}, \quad i,\ \alpha = 1,\ 2,\ 3. \tag{1}$$

The 3×3 matrix $\mathbf{B}$ is introduced by Ting (1986) as

$$\mathbf{B} = (\mathbf{R}^{\mathrm{T}} + \mathbf{pT})\mathbf{A}, \tag{2}$$

where $\mathbf{p} = \{p_1, p_2, p_3\}^{\mathrm{T}}$ and $\mathbf{A} = [\mathbf{a}_1, \mathbf{a}_2, \mathbf{a}_3]$ are the eigenvector and eigenvalue matrix of the following equation, respectively,

$$\{\mathbf{Q} + \mathbf{p}(\mathbf{R} + \mathbf{R}^{\mathrm{T}}) + \mathbf{p}^2\mathbf{T}\}\mathbf{a} = \mathbf{0}, \tag{3}$$

and $\mathbf{Q}$, $\mathbf{R}$ and $\mathbf{T}$ are stiffness matrices defined from the stiffness constants C_{ijkl} as

$$\mathbf{Q} = [Q_{ik}] = [C_{i1k1}], \quad \mathbf{R} = [R_{ik}] = [C_{i1k2}], \quad \mathbf{T} = [T_{ik}] = [C_{i2k2}], \qquad i,\ k = 1,\ 2,\ 3. \tag{4}$$

Denoting the eigenvectors with positive imaginary part as p_α, $\alpha = 1,\ 2,\ 3$, z_α in Eq. (1) are defined as

$$z_\alpha = x_1 + p_\alpha x_2 = \frac{1 - \mathrm{i}p_\alpha}{2} z + \frac{1 + \mathrm{i}p_\alpha}{2} \bar{z}, \qquad \alpha = 1,\ 2,\ 3. \tag{5}$$

The stress components can be calculated from Eq. (1) as

$$\sigma_{i1} = -\frac{\partial \phi_i}{\partial x_2} = -\mathbf{B}\langle\langle p_\alpha \rangle\rangle \left\{ f'_\alpha(z_\alpha) \right\} - \bar{\mathbf{B}}\langle\langle \bar{p}_\alpha \rangle\rangle \left\{ \bar{f}'_\alpha(\bar{z}_\alpha) \right\}, \tag{6a}$$

$$\sigma_{i2} = \frac{\partial \phi_i}{\partial x_1} = \mathbf{B}\left\{ f'_\alpha(z_\alpha) \right\} + \bar{\mathbf{B}} \left\{ \bar{f}'_\alpha(\bar{z}_\alpha) \right\}, \quad i,\ \alpha = 1,\ 2,\ 3. \tag{6b}$$

The double angle brackets stand for the diagonal matrix, i.e.,

$$\langle\langle p_\alpha \rangle\rangle = \begin{bmatrix} p_1 & 0 & 0 \\ 0 & p_2 & 0 \\ 0 & 0 & p_3 \end{bmatrix}. \tag{7}$$

Assuming the dislocation $\mathbf{b} = \{b_1, b_2, b_3\}^{\mathrm{T}}$ is located at $z_0 = x_{10} + \mathrm{i}x_{20}$ in the upper half plane, i.e., medium (1), of the bimaterial infinite plane (as shown in Fig. 1), the functions $f_\alpha(z_\alpha)$ in Eqs. (1), (6a) and (6b) can be found in Atkinson and Eftaxiopoulos (1991):

$$f_\alpha^{(1)}(z_\alpha^{(1)}) = \frac{1}{4\pi} \mathbf{M}_\alpha^{(1)} \mathbf{D}^{(1)} \mathbf{b}^{(1)} \ln(z_\alpha^{(1)} - z_{0\alpha}^{(1)}) + \frac{1}{4\pi} \mathbf{E}_\alpha \ln(z_\alpha^{(1)} - \bar{\mathbf{z}}_0^{(1)}), \tag{8}$$

$$f_\alpha^{(2)}(z_\alpha^{(2)}) = \frac{1}{4\pi} \mathbf{G}_\alpha \ln(z_\alpha^{(2)} - \mathbf{z}_0^{(1)}), \tag{9}$$

where

$$\mathbf{z}_0^{(1)} = \left\{ z_{01}^{(1)}, z_{02}^{(1)}, z_{03}^{(1)} \right\}^{\mathrm{T}}, \qquad \mathbf{M}^{(1)} = \mathbf{B}^{(1)^{-1}}, \qquad \mathbf{D}^{(1)} = -2\mathrm{i}(\mathbf{A}^{(1)}\mathbf{M}^{(1)} - \bar{\mathbf{A}}^{(1)}\bar{\mathbf{M}}^{(1)})^{-1},$$

and $\mathbf{M}_\alpha$, $\mathbf{E}_\alpha$, and $\mathbf{G}_\alpha$ stand for the α row of the matrix $\mathbf{M}$, $\mathbf{E}$, and $\mathbf{G}$, respectively, i.e., $\mathbf{M}_\alpha$, $\mathbf{E}_\alpha$, and $\mathbf{G}_\alpha$ are 1×3 row vectors. The superscripts (1) and (2) indicate material (1) and (2), respectively, and $\mathbf{E}$ and $\mathbf{G}$ are constants, depending on the dislocation density $\mathbf{b}$ and the elastic properties of media (1) and (2). They can be determined by solving the following linear equations:

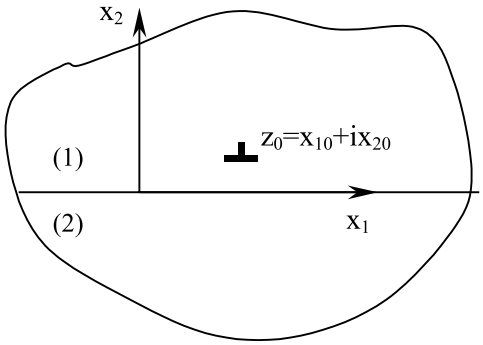

Fig. 1. Dislocation in bimaterial infinite plane.

$$\begin{bmatrix} -\bar{\mathbf{A}}^{(1)} & \mathbf{A}^{(2)} \\ -\bar{\mathbf{B}}^{(1)} & \mathbf{B}^{(2)} \end{bmatrix} \begin{Bmatrix} \bar{\mathbf{E}} \\ \mathbf{G} \end{Bmatrix} = \begin{Bmatrix} \bar{\mathbf{A}}^{(1)} \langle\langle \mathbf{M}^{(1)} \mathbf{D}^{(1)} \mathbf{b} \rangle\rangle \\ \bar{\mathbf{B}}^{(1)} \langle\langle \mathbf{M}^{(1)} \mathbf{D}^{(1)} \mathbf{b} \rangle\rangle \end{Bmatrix}. \tag{10}$$

Detailed derivation of Eq. (10) can be found in Atkinson and Eftaxiopoulos (1991). Although in that paper it was not specifically stated that their solution is applicable to the interface dislocation, our calculation yielded the same results from both Atkinson and Eftaxiopoulos (1991) and Qu and Li (1991) method for interface dislocations.

Because of the linearity of the stress fields of dislocations in the infinite bimaterial plane, we can express the stress components at $z = x_1 + \mathrm{i}x_2$ due to a dislocation $\mathbf{b} = \{b_1, b_2, b_3\}^{\mathrm{T}}$ at $z_0 = x_{10} + \mathrm{i}x_{20}$ as

$$\sigma_{ij}(x_1, x_2) = \mathbf{F}_{ij}(x_1, x_2, x_{10}, x_{20})\, \mathbf{b}(x_{10}, x_{20}), \tag{11}$$

where

$$\mathbf{F}_{ij}(x_1, x_2, x_{10}, x_{20}) = [f_{1ij}(x_1, x_2, x_{10}, x_{20}), f_{2ij}(x_1, x_2, x_{10}, x_{20}), f_{3ij}(x_1, x_2, x_{10}, x_{20})], \tag{12}$$

$$\mathbf{b}(x_{10}, x_{20}) = \{b_1(x_{10}, x_{20}), b_2(x_{10}, x_{20}), b_3(x_{10}, x_{20})\}^{\mathrm{T}}. \tag{13}$$

The physical meaning of f_{lij} is that they are the stress components σ_{ij} due to a unit dislocation $b_l = 1$. Therefore, we can calculate f_{1ij}, f_{2ij}, and f_{3ij} from Eqs. (6a) and (6b) by setting $\mathbf{b} = \{1, 0, 0\}^{\mathrm{T}}$, $\mathbf{b} = \{0, 1, 0\}^{\mathrm{T}}$, and $\mathbf{b} = \{0, 0, 1\}^{\mathrm{T}}$, respectively.

2.2. Dislocation solution in bimaterial half planes

Next, the dislocation solution in two different half plane configurations is formulated. The half plane configuration shown in Fig. 2 consists of an anisotropic infinite strip with thickness H and an anisotropic half plane. The free boundary is parallel to the material interface. The second half plane configuration is composed of two anisotropic infinite quarter planes with the free boundary perpendicular to the interface, as shown in Fig. 3. The basic idea of calculating the dislocation solution in the half plane is to apply a dislocation array along the free boundary of the half plane. The densities of the dislocation array are determined in such a way that the traction forces along the boundary due to the single dislocation and the dislocation array cancel out and thus the boundary is traction free, as shown in Figs. 2 and 3. For convenience, the half plane configuration in Fig. 2 is referred to as half plane A, and the one in Fig. 3 is referred to as half plane B.

Let's formulate the dislocation solution for half plane A first. Dislocation $\mathbf{b} = \{b_1, b_2, b_3\}^{\mathrm{T}}$ is located at an arbitrary point $z_0 = x_{10} + ix_{20}$. The geometry of a dislocation in the infinite strip can be decomposed into two geometries. The first one is a single dislocation located in the bimaterial infinite plane. The dashed line

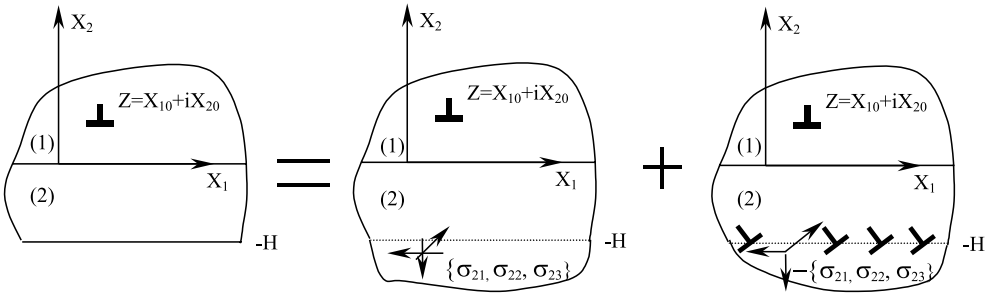

Fig. 2. Dislocation solution in half plane A: boundary parallel to interface.

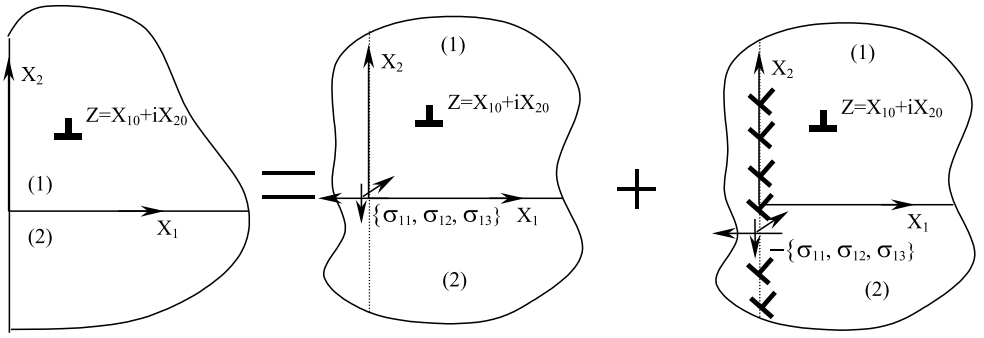

Fig. 3. Dislocation solution in half plane B: boundary perpendicular to interface.

stands for the boundary of the half plane, which is supposed to be traction free. The traction forces along the dashed line due to the single dislocation can be determined from Eq. (11):

$$\sigma_{ij}^{(s)}(x_1^{(2)}, -H) = \mathbf{F}_{ij}(x_1^{(2)}, -H, x_{10}, x_{20})\mathbf{b}(x_{10}, x_{20}), \tag{14}$$

where $ij = 21,\ 22$ and 23.

The second geometry is the infinite plane with a dislocation array along the supposed-to-be boundary of the half plane. To satisfy the traction free conditions along the half plane boundary, the traction forces along the dashed line in the second geometry should be the opposite of the traction forces in the first geometry. Suppose that the dislocation array is distributed from $-\infty$ to ∞, then the stress components along the dashed line due to the dislocation array can be calculated as

$$\sigma_{ij}(x_1^{(2)}, -H) = \int_{-\infty}^{\infty} \mathbf{F}_{ij}(x_1^{(2)}, -H, s, -H)\mathbf{b}(s, -H)\mathrm{d}s = -\sigma_{ij}^{(s)}(x_1^{(2)}, -H), \tag{15}$$

where $ij = 21,\ 22,$ and 23. Eq. (15) is a set of singular integral equations. Gaussian quadrature is adopted to solve these numerically. A summary of applying Gaussian quadrature to solve the singular integral equations is given in Appendix A. First, a variable transformation is introduced to transform the integral from $[-\infty,\ \infty]$ to $[-1,\ 1]$:

$$x_1^{(2)} = \frac{\tilde{t}}{1-\tilde{t}^2}, \quad \tilde{t} \in [-1, 1], \qquad s = \frac{\tilde{s}}{1-\tilde{s}^2}, \quad \tilde{s} \in [-1, 1]. \tag{16}$$

Substituting Eq. (16) into Eq. (15) yields

$$\sigma_{ij}(x_1^{(2)}, -H) = \int_{-1}^{1} \mathbf{F}_{ij}(x_1^{(2)}, -H, s, -H)\mathbf{b}(\tilde{s}, -H)\frac{1+\tilde{s}^2}{(1-\tilde{s}^2)^2}\mathrm{d}\tilde{s} = -\sigma_{ij}^{(s)}(x_1^{(2)}, -H). \tag{17}$$

Now, $\mathbf{b}(s, -H)$ should be zero at $s = -\infty,\ \infty$ because of the self equilibrium of the dislocation stress field. In other words, $\mathbf{b}(\tilde{s}, -H)$ is bounded at $\tilde{s} = -1,\ +1$. Therefore, case IV in Appendix A is adopted to solve Eq. (17). Accordingly, the dislocation densities may be written as

$$\mathbf{b}(\tilde{s}, -H) = W(\tilde{s})\tilde{\mathbf{b}}(\tilde{s}, -H), \quad W(\tilde{s}) = \sqrt{1-\tilde{s}^2}. \tag{18}$$

Substituting Eq. (18) into Eq. (17), the numerical form of the singular integral equations can be reduced to a set of algebraic equations having the following matrix forms (Appendix A):

$$\pi\left[\tilde{F}_{ij}(x_{1,k}^{(2)}, -H, s_m, -H)\right]\langle\langle \tilde{W}_m\rangle\rangle\tilde{\mathbf{b}}(\tilde{s}_m, -H) = \begin{Bmatrix} -\sigma_{21}^{(s)}(x_{1,k}^{(2)}, -H) \\ -\sigma_{22}^{(s)}(x_{1,k}^{(2)}, -H) \\ -\sigma_{23}^{(s)}(x_{1,k}^{(2)}, -H) \end{Bmatrix}, \tag{19}$$

where

$$[\tilde{F}_{ij}(x_{1,k}^{(2)}, -H, s_m, -H)] = \begin{bmatrix} \mathbf{F}_{21}(x_{1,k}^{(2)}, -H, s_m, -H) \\ \mathbf{F}_{22}(x_{1,k}^{(2)}, -H, s_m, -H) \\ \mathbf{F}_{23}(x_{1,k}^{(2)}, -H, s_m, -H) \end{bmatrix}, \tag{20}$$

$$\tilde{W}_m = W_m \frac{1+\tilde{s}_m^2}{(1-\tilde{s}_m^2)^2}, \quad x_{1,k}^{(2)} = \frac{\tilde{t}_k}{1-\tilde{t}_k^2}, \qquad s_m = \frac{\tilde{s}_m}{1-\tilde{s}_m^2}. \tag{21}$$

The integration points s_m, collocation points t_k, and weight coefficients W_m are calculated from case IV of Table 4 in Appendix A.

From Eq. (19), we can calculate the dislocations $\tilde{\mathbf{b}}(\tilde{s}_m, -H)$, which are related to the single dislocation $\mathbf{b}$. Denote the dislocation densities along the boundary of the half plane as $\tilde{\mathbf{b}}_1$ due to $\mathbf{b} = \{1,0,0\}^{\mathrm{T}}$, as $\tilde{\mathbf{b}}_2$ due to $\mathbf{b} = \{0,1,0\}^{\mathrm{T}}$, and as $\tilde{\mathbf{b}}_3$ due to $\mathbf{b} = \{0,0,1\}^{\mathrm{T}}$. Superposing the two elastic fields in Fig. 2, we can obtain the stress fields for a dislocation $\mathbf{b} = \{b_1, b_2, b_3\}^{\mathrm{T}}$ located at $z_0 = x_{10} + ix_{20}$ in the half plane:

$$\sigma_{ij}(x_1, x_2) = \tilde{\mathbf{F}}_{ij}(x_1, x_2, x_{10}, x_{20})\mathbf{b}(x_{10}, x_{20}), \tag{22}$$

where

$$\tilde{\mathbf{F}}_{ij}(x_1, x_2, x_{10}, x_{20}) = \left[\tilde{f}_{1ij}(x_1, x_2, x_{10}, x_{20}), \tilde{f}_{2ij}(x_1, x_2, x_{10}, x_{20}), \tilde{f}_{3ij}(x_1, x_2, x_{10}, x_{20})\right],$$

$$\tilde{f}_{lij}(x_1, x_2, x_{10}, x_{20}) = f_{lij}(x_1, x_2, x_{10}, x_{20}) + \pi\left[\tilde{F}_{ij}(x_1, x_2, s_m, -H)\right]\langle\langle \tilde{W}_m\rangle\rangle\tilde{\mathbf{b}}_l(\tilde{s}_m, -H) \quad l = 1,\ 2,\ 3. \tag{23}$$

The formulation for a dislocation in half plane B is only slightly different from that for half plane A. Since the boundary of half plane B is aligned with the x_2 axis, the stress components in Eqs. (14) and (15) should be $\sigma_{i1}(0, x_2)$, $i = 1,\ 2,\ 3$. These differences notwithstanding, one should be able to follow the procedure depicted above and obtain the dislocation solution for the half plane B easily.

2.3. Mixed-mode stress intensity factors for interface cracks and cracks parallel to the interface in bimaterial anisotropic half planes

In this section, the dislocation solutions for both half planes are applied to calculate the stress intensity factors for interface cracks and cracks parallel to the interface.

A crack of length $2a$ in half plane A is shown in Fig. 4a, which is parallel to the interface at a vertical distance of y_t. If $y_t = 0$, the crack is located at the interface and thus it turns into an interface crack. The origin of the coordinate system is located at the middle point of the interface crack. The crack in half plane B is parallel to the interface and perpendicular to the boundary, as shown in Fig. 4b. The vertical distance between the crack and the interface is y_t and the left crack tip A is located at a horizontal distance x_t from the boundary. Again, the crack becomes an interface crack when $y_t = 0$. We denote by T_{21}, T_{22}, and T_{23} the external load distributed along the crack surfaces. Only the tensile load T_{22} is studied in this paper. Both cracks can be modeled as a series of dislocations with dislocation densities $\mathbf{b}(s, y_t)$ in the half plane.

Considering the crack in half plane A, the tractions along the crack surfaces due to the dislocation series are

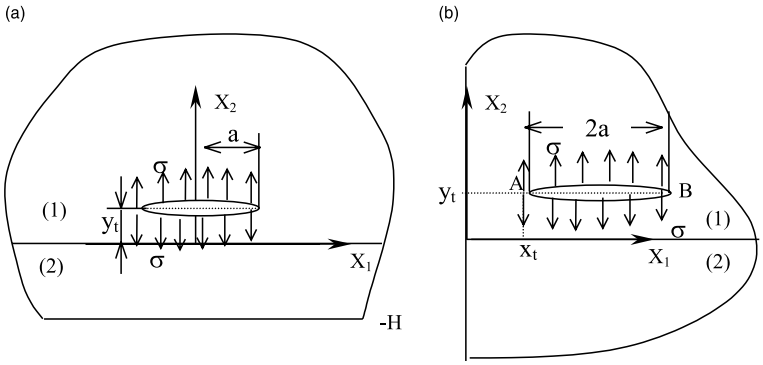

Fig. 4. Cracks in half plane A and B.

$$\sigma_{ij}(x_1,y_t)^{(d)}=\int_{-a}^{a}\tilde{\mathbf{F}}_{ij}(x_1,y_t,s,y_t)\mathbf{b}(s,y_t)\mathrm{d}s,\quad ij=21,\ 22,\ 23, \tag{24}$$

which should be equal to the opposite of the external loads T_{21}, T_{22} and T_{23}. Since both ends of the crack are singular, we use the case I Gaussian formula (see Appendix A) to solve Eq. (24). The $3(N-1)$ linear algebraic equations are

$$\pi a\tilde{\mathbf{F}}_{ij}(x_{1,k},y_t,s_m,y_t)\langle\langle W_m,W_m,W_m\rangle\rangle\tilde{\mathbf{b}}(s_m,y_t)=-T_{ij}(x_{1,k},y_t)\quad ij=21,\ 22,\ 23,\ k=1,\ 2,\ldots,\ N-1, \tag{25}$$

where

$$s_m=a\tilde{s}_m,\qquad x_{1,k}=a\tilde{t}_k,\qquad \tilde{\mathbf{b}}(\tilde{s}_m,y_t)=\frac{\mathbf{b}(\tilde{s}_m,y_t)}{\sqrt{1-\tilde{s}_m^2}}. \tag{26}$$

Here we assume the stress singularity at the interface crack tip is $1/\sqrt{r}$ because the oscillation index of interface crack is small ($\epsilon<0.03$) for the materials studied and the contact zone due to crack tip stress oscillation is very small ($\delta<10^{-4}$) for tensile loading.

In addition, the requirement that the crack surfaces physically come together at both ends imposes three additional equations:

$$\sum_{m=1}^{N}W_m\tilde{b}_l(\tilde{s}_m,y_t)=0,\quad l=1,\ 2,\ 3. \tag{27}$$

For the crack shown in Fig. 4b, Eq. (25) still applies except that the stress functions $\tilde{\mathbf{F}}_{ij}(x_{1,k},y_t,s_m,y_t)$ in Eq. (25) are the stress fields of a dislocation in half plane B and Eq. (26) becomes

$$s_m=x_t+a+a\tilde{s}_m,\qquad x_{1,k}=x_t+a+a\tilde{t}_k, \tag{28}$$

where $\tilde{s}_m$ and $\tilde{t}_k$ are also calculated from case I in Table 4.

Eqs. (25) and (27) enable us to calculate the dislocation densities $\mathbf{b}(\tilde{s}_m,0)$ at the N integration points. The crack-tip dislocation densities can be extrapolated from these N integration points as

$$\tilde{b}_l(1,y_t)=M_E\sum_{m=1}^{N}b_E\tilde{b}_l(\tilde{s}_m,y_t), \tag{29a}$$

for the right crack tip, and

$$\tilde{b}_l(-1, y_t) = M_E \sum_{m=1}^{N} b_E \tilde{b}_l(\tilde{s}_{N+1-m}, y_t), \tag{29b}$$

for the left crack tip (Hills et al., 1996), where $b_E = \sin[\pi(2m-1)(2N)/4N]/\sin[\pi(2m-1)/4N]$, $M_E = 1/N$, and $l = 1,\ 2,\ 3$.

The stress intensity factor $\mathbf{K}$ at the crack tip is related to the crack-tip dislocation densities as (see Appendix B)

$$\mathbf{K}(+1) = [K_{\mathrm{II}}, K_{\mathrm{I}}, K_{\mathrm{III}}] = \frac{\sqrt{\pi a}}{2} \mathrm{Re}\left[\mathbf{B}\left\{\mathbf{MD}\tilde{\mathbf{b}}(+1) + \delta(y_t)\sum_{j=1}^{3}\mathbf{E}_j(+1)\right\}\right], \tag{30a}$$

where Re[ ] stands for the real part of a complex variable and $\delta(y_t)$ is the Dirac delta function. $\mathbf{E}(+1)$ is solved from Eq. (10) with $\mathbf{b} = \tilde{\mathbf{b}}(+1)$ and $\mathbf{E}_j(+1)$ is the j column vector of $\mathbf{E}(+1)$. Similarly,

$$\mathbf{K}(-1) = [K_{\mathrm{II}}, K_{\mathrm{I}}, K_{\mathrm{III}}] = -\frac{\sqrt{\pi a}}{2} \mathrm{Re}\left[\mathbf{B}\left\{\mathbf{MD}\tilde{\mathbf{b}}(-1) + \delta(y_t)\sum_{j=1}^{3}\mathbf{E}_j(-1)\right\}\right]. \tag{30b}$$

Eqs. (30a) and (30b) give an explicit relation between the mixed-mode stress intensity factors and the crack tip dislocation densities. For the sake of clarity, a detailed derivation of Eqs. (30a) and (30b) is presented separately in Appendix B.

3. Results and discussions

The method presented above is implemented in a computer code for both bimaterial half planes. First, to validate this method, we choose the two materials to be identical. Under this condition, the bimaterial solution should reduce to the solution for homogeneous anisotropic materials. In this manner, it is easy to verify the solution because the analytical solution for a dislocation in a homogeneous anisotropic half plane is known (Atkinson and Eftaxiopoulos, 1991; Lee, 1990). Cross-ply composite laminates are studied in this paper. The elastic material properties for graphite/epoxy were taken from Salpekar's paper (Salpekar, 1993) and listed in Table 1. The fiber orientation θ° of the laminate is defined as the angle between the x_1 direction and the laminate's longitudinal direction. Also, x_2 is the normal direction of the laminate and the x_3 direction is determined by right-hand rule. A $0^\circ/90^\circ$ half plane means that the top material (1) is 0° and the bottom material (2) is 90°.

First, the convergence of the numerical integration is checked and the results for half plane A are listed in Table 2. A $45^\circ/45^\circ$ laminate is used in the calculation. The free boundary is located at $y = -1$ and the dislocation $\mathbf{b} = \{1, 0, 0\}^{\mathrm{T}}$ is located at $z_0 = 0$. Obviously, the stress components converge very well and agree with the analytic solution closely.

Table 3 gives the comparison of the present solution with the analytic solution for half plane B. The material is chosen to be $90^\circ/90^\circ$. We checked the stress components of eight points surrounding a dislo-

Table 1
Material properties for graphite/epoxy laminate

$E_{\mathrm{L}} = 134.45$ GPa, $E_{\mathrm{T}} = 11.03$ GPa, $E_{\mathrm{N}} = 11.03$ GPa
$G_{\mathrm{LT}} = 5.84$ GPa, $G_{\mathrm{LN}} = 5.84$ GPa, $G_{\mathrm{TN}} = 2.98$ GPa
$\mu_{\mathrm{LT}} = 0.301$, $\mu_{\mathrm{LN}} = 0.301$, $\mu_{\mathrm{TN}} = 0.49$

L is the longitudinal direction (fiber direction); T, the transverse direction, and N, the normal direction.

Table 2
Convergence of stresses for a dislocation in homogeneous anisotropic half plane A[a]

Stresses	$z = x_1 + ix_2$	Number of Integration Points N						Atkinson and Eftaxiopoulos (1991)
		10	50	100	150	200	250	
	1	1.6251	1.6333	1.6333	1.633	1.6333	1.6333	1.6333
σ_{21}	5	0.2732	0.2471	0.2547	0.255	0.255	0.255	0.255
	10	0.1009	0.0489	0.0613	0.0644	0.0652	0.0654	0.0655
	1	−0.1536	−0.1536	−0.1634	−0.1634	−0.1634	−0.1634	−0.1634
σ_{22}	5	0.0214	0.0214	0.0524	0.0521	0.0521	0.0521	0.0521
	10	−0.0293	−0.0293	0.0142	0.0109	0.0096	0.0091	0.0089
	1	−0.959	−0.9607	−0.9607	−0.9607	−0.9607	−0.9607	−0.9607
σ_{23}	5	−0.1854	−0.1706	−0.1717	−0.1717	−0.1717	−0.1717	−0.1717
	10	−0.0619	−0.0427	−0.0467	−0.0473	−0.0474	−0.0474	−0.0474

[a] Material: 45°/45°, $H = 1$; dislocation $\mathbf{b} = \{1,\ 0,\ 0\}^{\mathrm{T}}$ located at $z_0 = 0$.

Table 3
Comparison between present method and analytical solution of Atkinson and Eftaxiopoulos (1991) for half plane B[a]

$z = x_1 + ix_2$	Present			Analytical solution		
	σ_{11}	σ_{12}	σ_{22}	σ_{11}	σ_{12}	σ_{22}
0.5−0.5i	0.34	−0.1911	−1.9513	0.34	−0.1911	−1.9513
1−0.5i	0.2674	1.4793	−0.3698	0.2674	1.4793	−0.3698
1.5−0.5i	0.1905	−0.0981	1.2819	0.1905	−0.0981	1.2819
1.5	1.887	0	1.258	1.887	0	1.258
1.5+0.5i	0.1905	0.0981	1.2819	0.1905	0.0981	1.2819
1+0.5i	0.2674	−1.4793	−0.3698	0.2674	−1.4793	−0.3698
0.5+0.5i	0.34	0.1911	−1.9513	0.34	0.1911	−1.9513
0.5	−0.9815	0	−1.9629	−0.9815	0	−1.9629

[a] Material: 90°/90°, and dislocation $\mathbf{b} = \{0, 1, 0\}^{\mathrm{T}}$ located at $z_0 = 1$.

cation $\mathbf{b} = \{0, 1, 0\}^{\mathrm{T}}$ at $z_0 = 1$. The number of integration points, N, is 300. Again, we obtained excellent agreements between these two solutions.

Next, let's study the mixed-mode stress intensity factors for half planes A and B. Fig. 5a displays the three modes of stress intensity factors for interfacial cracks with normalized crack length from 0.5 to 5. Fig. 5a gives the mode-I stress intensity factor for interfacial cracks in half plane A of different material combinations. The stress intensity factors are normalized as $\bar{\mathbf{K}} = \mathbf{K}/\sigma\sqrt{\pi a}$, where σ is the external tensile load. Fig. 5b and c gives the mode-II and mode-III mode mixity. The mode mixities ψ are defined as

$$\psi_{\mathrm{II}} = \tan^{-1}\left(\frac{K_{\mathrm{II}}}{K_I}\right), \qquad \psi_{\mathrm{III}} = \tan^{-1}\left(\frac{K_{\mathrm{III}}}{K_I}\right),$$

and the ratio between mode-I components and mode-II or mode-III components is expressed. It can be seen in these plots that material combinations affect both the mode-I stress intensity factors and the mode mixities. Homogeneous 90° material has the highest mode-I stress intensity factor K_{I}, 90°/0° and homogeneous 0° material give the lowest K_{I}. As for mode-II mode mixities, bimaterials have lower mode-II mode mixities compared with their homogeneous counterparts. Only 45°/ − 45° and 45° homogeneous materials display mode-III mode-mixities. Again, the bimaterial 45°/ − 45° has smaller mode-III mode mixity than the homogeneous materials. The non-zero mode-mixities indicate that cracks in bimaterial and homogeneous anisotropic are prone to propagate away from the original crack orientation.

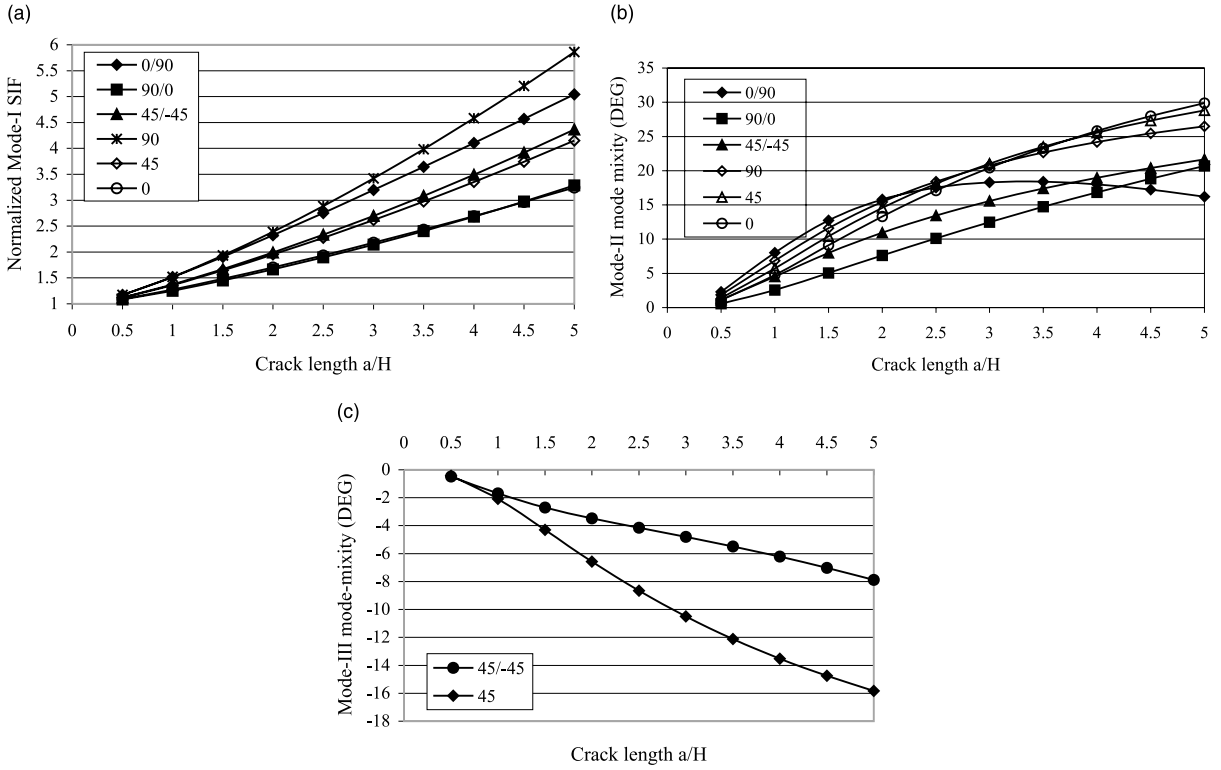

Fig. 5. Stress intensity factors for interfacial cracks with different lengths in half plane A.

Fig. 6 gives the stress intensity factors and mode-mixities for cracks parallel to the material interface. The vertical distance between the crack tip and the interface is y_t, as shown in Fig. 4a. We compare the stress intensity factors of $0°/90°$ material with that of homogeneous $90°$ materials. The normalized crack length is $a/H = 2$ and the vertical distance y_t is normalized by the distance H between the free boundary and the material interface. The stress intensity factor and mode-mixity curves for the homogeneous $90°$ material are smooth, however, those for the $0°/90°$ bimaterial are not continuous across the material interface and display drastic changes in the area very close to the material interface. When the crack is far away from the interface, the stress intensity factors and mode-mixities for both materials are almost identical. In order to give a clear picture of the changes of $\bar{K}_{\mathrm{I}}$ and ψ_{II} around the interface, a zoom-in on Fig. 6a and b near the interface is shown in Fig. 6c and d, respectively. The powerwise increase/decrease in K_{I} as the cracks approach the interface was also observed by Atkinson and Eftaxiopoulos (1991) for cracks in a bimaterial infinite plane. The stress intensity factors K_{I} for cracks in half plane B and infinite plane have the same powerwise behavior, as shown in Fig. 7.

The effect of the interface on the stress intensity factors of cracks in half plane B is also studied and the results are shown in Fig. 7. The material is chosen to be $90°/0°$ and the horizontal distance between crack tip A and the free boundary is $x_t = a/4$. Again, the mode-I stress intensity factor $\bar{K}_{\mathrm{I}}$ is larger when the crack is located in the $0°$ materials and has a big drop across the interface from $0°$ to $90°$. Also shown in the plot are $\bar{K}_{\mathrm{I}}$ for a $90°/0°$ infinite plane. These two curves are almost parallel indicating the presence of free boundary increase $\bar{K}_{\mathrm{I}}$. Unlike cracks in half plane A, cracks in half plane B remain mode-I dominated despite the free boundary and the material heterogeneity.

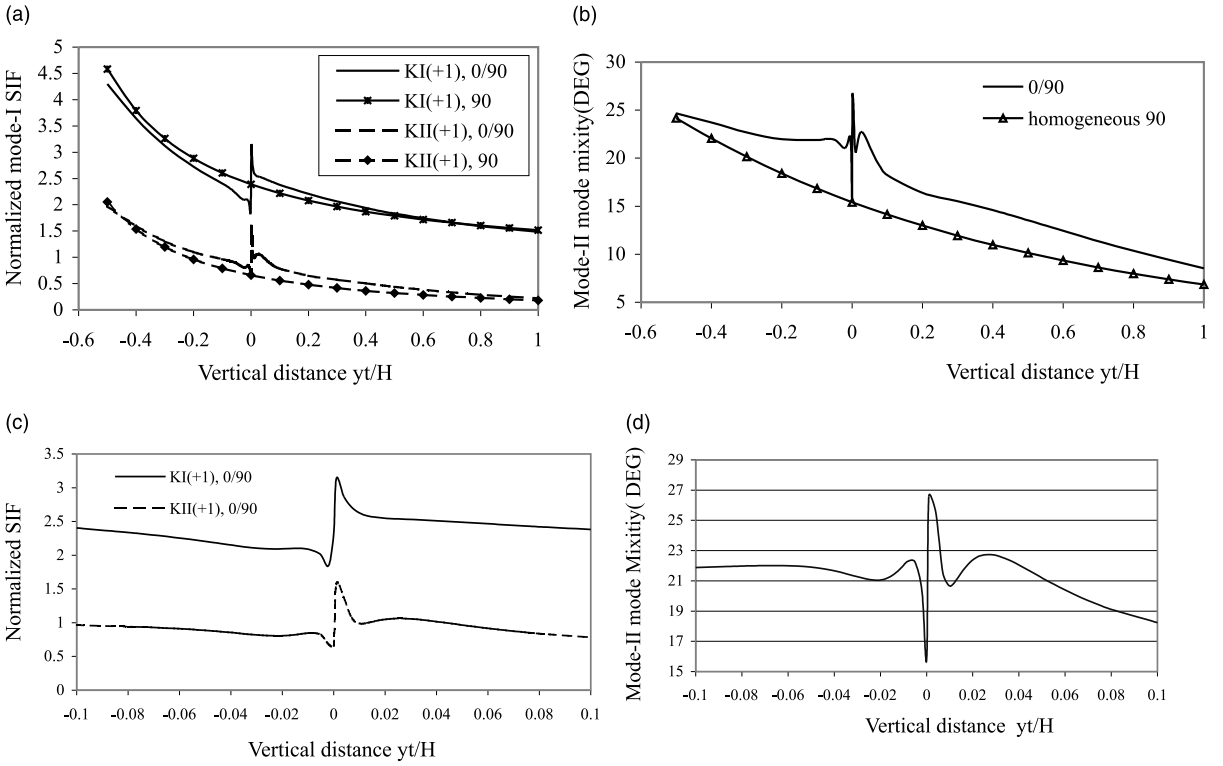

Fig. 6. Stress intensity factors for cracks parallel to the material interface in half plane A. y_t is the vertical distance between the crack tip and the interface. Crack length $a/H = 2$.

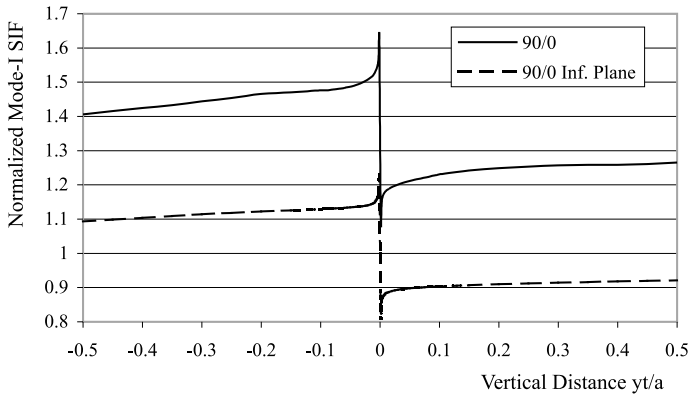

Fig. 7. Mode-I stress intensity factors across the material interface for cracks in bimaterial half plane B. The horizontal distance between the crack tip A and the boundary is $x_t = a/4$.

To study how the stress intensity factors change with the crack length a, we fixed the crack tip at a distance of $x_t = 1$ from the free boundary and varied the crack length. The calculation results for interfacial cracks in different materials are plotted in Fig. 8. Again the cracks are mode-I dominated and the variation

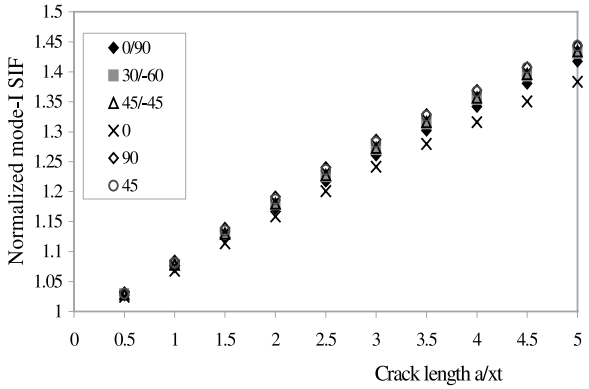

Fig. 8. Normalized mode-I stress intensity factors for interfacial cracks in bimaterial half plane B with different crack lengths.

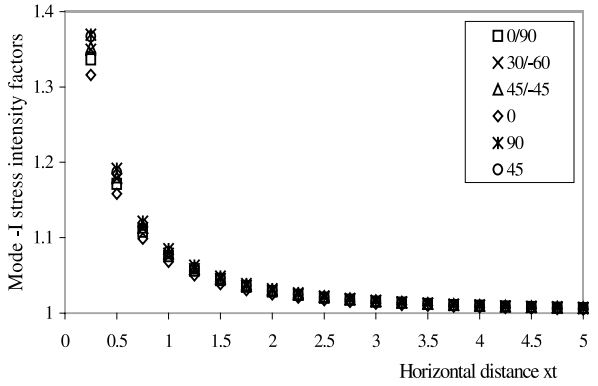

Fig. 9. Normalized mode-I stress intensity factors for interfacial cracks in bimaterial half plane B at different horizontal distances from the boundary.

in $\bar{K}_{\mathrm{I}}$ for different materials increases slightly as the crack length increases. Even for the longest crack considered, the mode-I stress intensity factors for different materials are close to each other.

Finally, we investigated the influence of the free boundary on the stress intensity factors. The interfacial crack length is kept at $a = 2$. As shown in Fig. 9, the mode-I stress intensity factors are not very different for all bimaterials and homogeneous materials and converge to the same value when the crack tip A is far away from the free boundary. The mode-II stress intensity factors are small enough to be neglected.

4. Conclusions

Dislocation solutions in two different bimaterial half planes are derived based on the analytical dislocation solution in a bimaterial infinite plane. The convergence and accuracy of the numerical integration method are verified by setting the two materials to be identical and comparing the numerical results with the analytical solution for the homogeneous case. The dislocation solution is then applied to calculate the mixed-mode stress intensity factors for interfacial cracks or cracks parallel to the interface in both half planes. Based on the calculation results, the following conclusions can be drawn:

(1) For a half plane with free boundary parallel to the interface, i.e., half plane A, different material combinations yield different stress intensity factors for cracks having the same geometries. Moreover, these cracks could involve all three modes of fracture.

(2) In half plane A, the mode mixities of cracks at the interface are much smaller than those of cracks located near the interface.

(3) For a half plane with free boundary perpendicular to the interface, i.e., half plane B, the cracks are mode-I dominated and do not change very much with the material.

(4) The free boundary of half plane B only increases the mode-I stress intensity factors of the cracks but does not make the cracks mixed-mode.

(5) In both half plane A and half plane B, the mode-I stress intensity factors changes abruptly across the interface.

Acknowledgements

The financial support of the National Rotorcraft Technology Center through CERT, Grant NCC2-945, of the Office of Naval Research, Ship Structures S&T Division, Grant N00014-90-J-1995, and of the Air Force Office of Scientific Research, Grant F49620-98-1-0384, and the interest and encouragement of the Grant Monitors, Dr. G. Anderson, Dr. T.K. O'Brien, Dr. Y.D.S. Rajapakse, Dr. Brian Sanders and Dr. Ozden Ochoa, are all gratefully acknowledged.

Appendix A. Gaussian quadrature for singular integral equations

In this appendix, we give a general summary of applying Gaussian quadrature to solve the singular integral equations with Cauchy kernel that are formulated in this analysis. The singular integral equations for these crack problems have the following format:

$$I(t) = \int_{-l_1}^{-l_2} b(s) f(t,s)\,\mathrm{d}s. \tag{A.1}$$

where s and t are the coordinates along the crack surface, and l_1 and l_2 are the crack tips. Also, $f(t,s)$ is a singular function with Cauchy kernel, i.e.,

$$f(t,s) = \frac{F(t,s)}{t-s}, \tag{A.2}$$

where $F(t,s)$ is a continuous smooth function. First, Eq. (A.1) is normalized so that the crack is lying along $[-1,+1]$

$$\tilde{t} = \frac{2t-(l_1+l_2)}{l_2-l_1}, \qquad \tilde{s} = \frac{2s-(l_1+l_2)}{l_2-l_1}. \tag{A.3}$$

Substituting Eqs. (A.2) and (A.3) into Eq. (A.1) yields

$$I(t) = \pi\frac{l_2-l_1}{2}\left[\frac{1}{\pi}\int_{-1}^{+1} b(\tilde{s}) f(t,s)\mathrm{d}\tilde{s}\right] = \pi\frac{l_2-l_1}{2}\left[\frac{1}{\pi}\int_{-1}^{+1} b(\tilde{s})\frac{F(t,s)}{t-s}\mathrm{d}\tilde{s}\right]. \tag{A.4}$$

The integral inside the bracket is a singular integral with Cauchy kernel and will be numerically solved by Gaussian quadrature.

In Eq. (A.4), $b(\tilde{s})$ are the densities of the continuous dislocation array, which is employed to model the crack. Different types of singularity of the crack tip dislocation is built into the dislocation density by expressing $b(\tilde{s})$ as

Table 4
Gaussian quadrature formulae for Cauchy kernels

Case	$\omega(\tilde{s})$	$\tilde{s}_m$	$\tilde{t}_k$	n	W_m
I	$(1-\tilde{s}^2)^{-1/2}$	$\cos(\pi(2m-1)/2N)$	$\cos(\pi(k/N))$	1	$1/N$
II	$(1-\tilde{s})^{+1/2}(1+\tilde{s})^{-1/2}$	$\cos(\pi 2m/(2N+1))$	$\cos(\pi(2k-1)/(2N+1))$	0	$2(1-\tilde{s}_m)/(2N+1)$
III	$(1-\tilde{s})^{-1/2}(1+\tilde{s})^{+1/2}$	$\cos(\pi(2m-1)/(2N+1))$	$\cos(\pi 2k/(2N+1))$	0	$2(1+\tilde{s}_m)/(2N+1)$
IV	$(1-\tilde{s}^2)^{+1/2}$	$\cos(\pi m/(N+1))$	$\cos(\pi(2k-1)/(2N+1))$	-1	$(1-\tilde{s}_m^2)/(N+1)$

$$b(\tilde{s}) = \omega(\tilde{s})\tilde{b}(\tilde{s}). \tag{A.5}$$

The function $\tilde{b}(\tilde{s})$ is a smooth continuous function and $\omega(\tilde{s})$ is a weight function of the form:

$$\omega(s) = (1-\tilde{s})^{\gamma}(1+\tilde{s})^{\rho}. \tag{A.6}$$

It can be proved (Muskhelishvili, 1953; Stroh, 1958) that the exponents γ and ρ must be either $+1/2$ or $-1/2$ for isotropic and anisotropic materials. It is also true for anisotropic bimaterials if the oscillation index ϵ is neglected. As a result, four separate classes of singular integral equations arise, depending on the behavior of the density $b(\tilde{s})$ at the end points. These are

$$\begin{array}{lll} \textit{Case I} & b(\tilde{s}) \text{ singular at both ends} & : \ \gamma=-1/2, \quad \rho=-1/2; \\ \textit{Case II} & b(\tilde{s}) \text{ singular at } \tilde{s}=-1 \text{ and bounded at } \tilde{s}=+1 & : \ \gamma=+1/2, \quad \rho=-1/2; \\ \textit{Case III} & b(\tilde{s}) \text{ bounded at } \tilde{s}=-1 \text{ and singular at } \tilde{s}=+1 & : \ \gamma=-1/2, \quad \rho=+1/2; \\ \textit{Case IV} & b(\tilde{s}) \text{ bounded at both ends} & : \ \gamma=+1/2, \quad \rho=+1/2. \end{array} \tag{A.7}$$

The general strategy is to employ the Gaussian quadrature formulae to reduce equations of the type in the bracket of Eq. (A.4) to a set of $N-n$ algebraic equations having the form:

$$I(t_k) = \frac{1}{\pi}\int_{-1}^{+1} b(\tilde{s})f(t,s)\mathrm{d}\tilde{s} = [f(t_k,s_m)]\langle\langle W_m\rangle\rangle\left\{\tilde{b}(\tilde{s}_m)\right\}, \tag{A.8}$$

where

$$t_k = \frac{l_2(1+\tilde{t}_k)+l_1(1-\tilde{t}_k)}{2}, \quad s_m = \frac{l_2(1+\tilde{s}_m)+l_1(1-\tilde{s}_m)}{2}, \qquad k=1,\ 2,\ldots,\ N-n,$$
$$m=1,\ 2,\ldots,\ N. \tag{A.9}$$

The integer n depends on the combination of end point behavior anticipated, and is included in Table 4; W_m are the weight coefficients appropriate to the quadrature formulae employed. The coordinates of the integration points $\tilde{s}_m$, and the collocation points $\tilde{t}_k$, are also given in Table 4.

Applying to crack problems, case I is employed for crack closed at both ends, case II and III are for surface break cracks such as edge cracks, and case IV is employed in this paper to solve the dislocation densities along the traction-free boundary of the half planes.

A more detailed derivation of the numerical quadrature schemes for the solution of singular integral equations can be found in Hills et al. (1996).

Appendix B. Evaluation of the stress intensity factors from the crack tip dislocation densities

The singularity of the crack tip stresses is contributed by the first term at the right hand side of Eq. (23), as the second one is not singular. Since the first term $f_{lij}(x_1,x_2,x_{10},x_{20})$ is exactly the same as the stresses of the dislocation in an infinite plane, the relationship between the stress intensity factors and the dislocation

densities are the same for both infinite plane and half planes. Assuming that the crack is located at material (1) or the interface, we substitute the derivatives of Eq. (8) into Eqs. (6a) and (6b) and yield the stress components due to a dislocation located at z_0:

$$\sigma_{i1} = -2\,\mathrm{Re}\left[\mathbf{B}\langle\langle p_\alpha\rangle\rangle\left\{\frac{1}{4\pi}\mathbf{M}_\alpha^{(1)}\mathbf{D}^{(1)}\mathbf{b}^{(1)}\frac{1}{z_\alpha^{(1)}-z_{0\alpha}^{(1)}}+\frac{1}{4\pi}\mathbf{E}_\alpha\frac{1}{z_\alpha^{(1)}-\bar{\mathbf{z}}_0^{(1)}}\right\}\right], \tag{B.1a}$$

$$\sigma_{i2} = 2\,\mathrm{Re}\left[\mathbf{B}\left\{\frac{1}{4\pi}\mathbf{M}_\alpha^{(1)}\mathbf{D}^{(1)}\mathbf{b}^{(1)}\frac{1}{z_\alpha^{(1)}-z_{0\alpha}^{(1)}}+\frac{1}{4\pi}\mathbf{E}_\alpha\frac{1}{z_\alpha^{(1)}-\mathbf{z}_0^{(1)}}\right\}\right], \quad \alpha = 1,\ 2,\ 3. \tag{B.1b}$$

Suppose that the crack is parallel to the interface at a vertical distance y_t, the stress intensity factors at the crack tip $x_1 = a$ are related to the stresses as

$$\mathbf{K} = \{K_{\mathrm{II}}, K_{\mathrm{I}}, K_{\mathrm{III}}\}^{\mathrm{T}} = \lim_{x_1\to a}\sqrt{2\pi(a-x_1)}\sigma_{i2}(x_1, y_t). \tag{B.2}$$

In order to obtain the stresses due to the dislocation array along the crack surface, we replace $\mathbf{b}^{(1)}$ by $\mathbf{b}^{(1)}(s)\,\mathrm{d}s$ in Eq. (B.1b) and integrate with respect to s from $s = -a$ to $s = a$. Substituting the stress components into Eq. (B.2) gives

$$\mathbf{K}(x_1 = a) = \{K_{\mathrm{II}}, K_{\mathrm{I}}, K_{\mathrm{III}}\}^{\mathrm{T}} = \lim_{x_1\to a}\sqrt{2\pi(a-x_1)}2\,\mathrm{Re}\left[\mathbf{B}\left\{\frac{1}{4\pi}\mathbf{M}^{(1)}\mathbf{D}^{(1)}\int_{-a}^{a}\frac{\mathbf{b}^{(1)}(s)}{x_1-s}\mathrm{d}s + \frac{1}{4\pi}\int_{-a}^{a}\mathbf{E}_\alpha(s)\frac{1}{(x_1-s)+(P_\alpha-\mathbf{P})y_t}\mathrm{d}s\right\}\right], \tag{B.3}$$

where $\mathbf{E}_\alpha(s)$ are related to $\mathbf{b}^{(1)}(s)$. If the crack is located away from the interface, i.e., $y_t \neq 0$, the second term in Eq. (B.3) is not singular as $x_1 \to s$, and thus will not contribute to the crack tip stress intensity factors. However, if the crack is an interface crack, i.e., $y_t = 0$, then the second term is also singular. Using the Dirac delta function, Eq. (B.3) can be expressed as

$$\mathbf{K}(x_1 = a) = \lim_{x_1\to a}\sqrt{2\pi(a-x_1)}2\,\mathrm{Re}\left[\mathbf{B}\left\{\frac{1}{4\pi}\mathbf{M}_\alpha^{(1)}\mathbf{D}^{(1)}\int_{-a}^{a}\frac{\mathbf{b}^{(1)}(s)}{x_1-s}ds + \frac{1}{4\pi}\delta(y_t)\sum_{j=1}^{3}\int_{-a}^{a}\mathbf{E}_j(s)\frac{1}{x_1-s}\mathrm{d}s\right\}\right]. \tag{B.4}$$

Introducing variable transformation $x_1 = ta$, and $s = \tilde{s}a$, Eq. (B.4) becomes

$$K(+1) = \sqrt{2\pi a}2\,\mathrm{Re}\left[\mathbf{B}\left\{\frac{1}{4\pi}\mathbf{M}_\alpha^{(1)}\mathbf{D}^{(1)}\lim_{t\to+1}\sqrt{1-t}\int_{-1}^{1}\frac{\mathbf{b}^{(1)}(\tilde{s})}{t-\tilde{s}}\mathrm{d}\tilde{s} + \frac{1}{4\pi}\delta(y_t)\sum_{j=1}^{3}\lim_{t\to+1}\sqrt{1-t}\int_{-1}^{1}\mathbf{E}_j(\tilde{s})\frac{1}{t-\tilde{s}}\mathrm{d}\tilde{s}\right\}\right]. \tag{B.5}$$

According to Hills et al. (1996), the limiting value of the first integral is $\pi\tilde{b}(+1)/\sqrt{2}$. Similarly, the limiting value of the second integral is $\pi\mathbf{E}_j(+1)/\sqrt{2}$. Thus, we have the relationship between the stress intensity factors and dislocation densities as following:

$$\mathbf{K}(+1) = [K_{\mathrm{II}}, K_{\mathrm{I}}, K_{\mathrm{III}}] = \frac{\sqrt{\pi a}}{2}\,\mathrm{Re}\left[\mathbf{B}\left\{\mathbf{MD}\tilde{\mathbf{b}}(+1) + \delta(y_t)\sum_{j=1}^{3}\mathbf{E}_j(+1)\right\}\right]. \tag{B.6a}$$

Similarly, the stress intensity factors at the crack tip $\tilde{s} = -1$ are

$$\mathbf{K}(-1) = [K_{\mathrm{II}}, K_{\mathrm{I}}, K_{\mathrm{III}}] = -\frac{\sqrt{\pi a}}{2}\,\mathrm{Re}\left[\mathbf{B}\left\{\mathbf{MD}\tilde{\mathbf{b}}(-1) + \delta(y_t)\sum_{j=1}^{3}\mathbf{E}_j(-1)\right\}\right]. \tag{B.6b}$$

References

Atkinson, C., Eftaxiopoulos, D.A., 1991. Interaction between a crack and a free or welded boundary in media with arbitrary anisotropy. Int. J. Fract. 50, 159–182.

Civelek, M.B., Erdogan, F., 1982. Crack problems for a rectangle plate and an infinite strip. Int. J. Fract. 19, 139–159.

Eshelby, J.D., Read, W.T., Shockley, W., 1953. Anisotropic elasticity with applications to dislocation theory. Acta Meta. 1, 251–259.

Hills, D.A., Kelly, P.A., Di, D.N., Korsunsky, A.M., 1996. Solution of Crack Problems; the Distributed Dislocation Technique. Kluwer, UK.

Huang, H., Kardomateas, G.A., 1999. Single-edge and double-edge cracks in a fully anisotropic strip. J. Engng. Mater. Technol. ASME Trans. 121 (4), 422–429.

Jagannadham, K., Marcinkowski, M.J., 1979. Surface dislocation model of a finite stressed solid. Mater. Sci. Engng. 38, 259–270.

Lee, J.C., 1990. Analysis of a fiber bridged crack near a free surface in ceramic matrix composites. Eng. Fract. Mech. 37 (1), 209–219.

Muskhelishvili, N.I., 1953. Some basic problems of the mathematical theory of elasticity. P. Noordhoff Ltd., Groningen, Holland.

O'Brien, T.K., Hooper, S.J., 1993. Local delamination in laminates with angle ply matrix cracks. Part I: Tension tests and stress analysis. In: Stinchcomb, W.W., Ashbaugh, N.E. (Eds.), Composite Materials: Fatigue and Fracture, vol. 4, ASTM STP 1156,. American Society for Testing and Materials, Philadelphia, pp. 491–506.

Qian, W., Sun, C.T., 1997. Calculations of stress intensity factors for interlaminar cracks in composite laminates. Composite Sci. Technol. 57, 637–650.

Qu, J., Li, Q., 1991. Interfacial dislocation and its applications to interface cracks in anisotropic bimaterials. J. Elast. 26, 169–195.

Salpekar, S.A., 1993. Analysis of delamination in cross-ply laminated initiating from impact induced matrix cracking. J. Composite Technol. Res. JCTRER 15 (2), 88–94.

Stroh, A.N., 1958. Dislocations and cracks in anisotropic elasticity. Philos. Mag. 7, 625–646.

Suo, Z., 1990. Delamination specimens for orthotropic materials. J. Appl. Mech. 57, 627–634.

Suo, Z., Hutchinson, J.W., 1990. Interface crack between two elastic layers. Int. J. Fract. 43, 1–18.

Ting, T., 1986. Explicit solution and invariance of the singularities at an interface crack in anisotropic composites. Int. J. Solids Struct. 22 (9), 965–983.